ChemComm

COMMUNICATION

View Article Online
View Journal | View Issue

Cite this: *Chem. Commun.*, 2024, **60**, 14463

Received 13th September 2024,
Accepted 2nd November 2024

DOI: 10.1039/d4cc04734f

rsc.li/chemcomm

Uncovering the unusual anodic current during tetrafluoroborate anion deintercalation from a graphite cathode in ethylene carbonate†

Haibo Liu,[ab] Yunju Wang,[c] Guobao Xu *[ab] and Hongyu Wang*[c]

During the deintercalation of ethylene carbonate (EC)-solvated tetrafluoroborate anions (BF_4^-) from a graphite cathode, an unusual anodic counter current was observed. The generation of counter-current is revealed to stem from the interaction between EC and BF_4^-, which provides new clues to the often-overlooked C–H···anion weak interactions in dual-ion battery (DIB) or other battery electrolyte research.

Achieving, identifying, and controlling electrochemical ion-solvent cointercalation are of importance in the field of electrochemical energy storage, particularly, in order to enable post-lithium cell chemistries.[1,2] In DIBs, anion–graphite intercalation compounds (AGICs) are usually employed as cathode materials. Anions intercalate from electrolyte solutions into graphite electrodes during the charge process, whereas they deintercalate from graphite into electrolyte solutions during the discharge process, corresponding to the anodic and cathodic currents, respectively.[3–5] However, in the case of BF_4^- solvated by EC, a surprisingly unusual anodic current peak sprouts out during the deintercalation of BF_4^- from the graphite cathode.[6] This phenomenon may be closely related to the following two reasons. First, EC solvent inversely flows from the electrolyte solution into the graphite electrode during the anion deintercalation from graphite into the solution; second, the strong affinity between EC and the anion leads to some BF_4^- accompanying EC back-flows into graphite. As for the first reason, a similar case may be found in the solution of $LiPF_6$ dissolved in ethyl methyl carbonate.[7] But counter current during discharge never appears. Therefore, the second reason must be an indispensable prerequisite to incur the unusual anodic current.

To test the above assumption, we tailor the solvation state of BF_4^- in the electrolyte solution and then correlate it with the generation of unusual anodic current at the graphite cathode in this study. Two series of EC solutions, including those dissolving the ionic liquid of 1-butyl-3-methylimidazolium tetrafluoroborate ($BMIMBF_4$) or the mixed salts of both tetraethylammonium tetrafluoroborate ($TEABF_4$) and hexafluorophosphate ($TEAPF_6$), are applied in the activated carbon/graphite capacitors. The anion–solvent co-intercalation of graphite cathode and multiple signal responses of counter-current is confirmed by X-ray diffraction (XRD), electrochemical dilatometry (ECD), and electrochemical quartz crystal microbalance (EQCM). Moreover, by analysing two-dimensional nuclear magnetic resonance (2D NMR) results, the reverse current can be attributed to the interaction between EC and BF_4^-. This work will help researchers reassess weak interactions in electrolytes and provide new insights into the formulation design of electrolytes for DIBs.

To verify that the unique combination of EC and BF_4^- is a prerequisite to generating counter current, we gradually added EC into the ionic liquid of $BMIMBF_4$ and then tested the performance of the graphite cathode in the corresponding electrolyte solutions. The reliability of activated carbon quasi-reference electrodes (AC-QRE) has been demonstrated previously.[8] As shown in Fig. 1, the counter current does not appear in the case of ionic liquid free of solvent. Instead, the redox peaks stand for reversible storage of "naked" BF_4^- in graphite electrodes. If the content of EC is less than that of $BMIMBF_4$, the current peaks become weaker with the addition of EC, which implies that EC may suppress the intercalation of BF_4^-. Moreover, there is no counter current at all during the cathodic scan. Once the molar ratio of [EC]/[$BMIMBF_4$] exceeds 1, a significant counter-current peak can be observed. As more and more EC is introduced into the solution, the concentration of BF_4^- decreases, and the polarization between the anodic and cathodic current peaks gets larger. Accordingly, the counter current looks less pronounced.

The effect of the addition of EC into the ionic liquid on BF_4^- intercalation into graphite electrodes can be manifested by the *ex situ* XRD results of graphite electrodes recovered from the

[a] *State Key Laboratory of Electroanalytical Chemistry, Changchun Institute of Applied Chemistry, Chinese Academy of Sciences, 5625 Renmin Street, Changchun 130022, China. E-mail: guobaoxu@ciac.ac.cn*
[b] *School of Applied Chemistry and Engineering, University of Science and Technology of China, Hefei 230026, China*
[c] *Key Laboratory of UV Light Emitting Materials and Technology, Ministry of Education, Northeast Normal University, 5628 Renmin Street, Changchun 130024, China. E-mail: hongyuwang@aliyun.com*

† Electronic supplementary information (ESI) available. See DOI: https://doi.org/10.1039/d4cc04734f

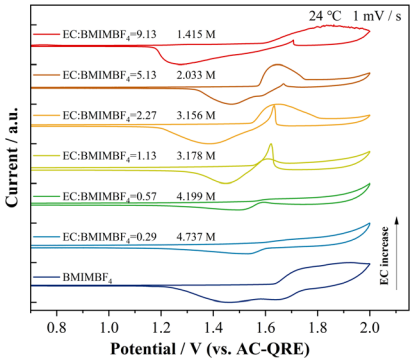

Fig. 1 Cyclic voltammograms of graphite electrodes in the electrolyte solutions of $BMIMBF_4$-EC in the initial cycle.

AC/graphite cells which were charged to 3.5 V (the specific charge/discharge curves are shown in Fig. S1, ESI†). As shown in Fig. 2 (AGICs parameters are shown in Table S1, ESI†), the graphite electrode charged in the neat ionic liquid demonstrates diffraction peaks corresponding to AGICs, while the (002) diffraction peak of the original graphite (at 26.5°) is absent, which means that the anion can adequately intercalate into graphite. In contrast, as EC is added into $BMIMBF_4$, little by little, say, the molar ratios of [EC]/[$BMIMBF_4$] amount to 0.57 or 0.29 in the electrolyte solutions, the (002) diffraction peak of the original graphite begins to dominate in the *ex situ* XRD patterns although there are some parasite peaks standing for the formation of AGICs. This indicates that the intercalation of BF_4^- into graphite is suppressed somehow. When there is sufficient EC in the electrolyte solutions, for example, the molar ratios of [EC]/[$BMIMBF_4$] are over 1, the (002) diffraction peak of the original graphite becomes apparently weaker than the peaks of AGICs. The stronger intensities of these diffraction peaks of AGICs imply that considerable capacities of the anion intercalate into graphite. These XRD results agree with the trend observed in Fig. 1.

In situ XRD characterizations of graphite cathode in AC/graphite capacitors may shed more light on the formation and transformations between AGICs. As shown in Fig. S2 (ESI†), for all electrolyte solutions, the anion storage in graphite electrode takes place, as evidenced by the emergence and growth of diffraction peaks of AGICs during the charging process. In contrast, the weakening and disappearance of these peaks during the discharge process occurs. From the *in situ* XRD patterns in Fig. S2 (ESI†), the intercalation gallery heights (IGHs) or stage numbers (SNs) of the AGICs can be calculated according to the methods introduced before.[9] These key parameters are plotted with respect to the voltages of AC/graphite cells in Fig. S3 and S4 (ESI†). Unfortunately, the signs for counter-current cannot be detected at all. This insensitivity can be ascribed to the limitation of the constant-voltage control on the cells during *in situ* XRD measurements, which cannot catch up with the instantaneous rise-up of counter current. Table 1 just lists the SNs and IGHs of AGICs corresponding to the AC/graphite cells charged to 3.5 V. The IGHs of AGICs obtained in EC-added solutions (0.807 to 0.817 nm) are apparently larger than those obtained in the neat ionic liquid (0.616 nm). This result strongly supports that the solvent of EC co-intercalates with BF_4^- into the graphite.

Table 1 Parameters of the anion–graphite intercalation compounds at 3.5 V

Electrolyte solution	Basal repeat length along C nm^{-1}	SN	IGH/nm
$BMIMBF_4$	1.666	4.14	0.614
EC:$BMIMBF_4$ = 0.29	2.122	4.92	0.809
EC:$BMIMBF_4$ = 0.57	2.301	5.40	0.807
EC:$BMIMBF_4$ = 1.13	2.014	4.59	0.811
EC:$BMIMBF_4$ = 5.13	1.923	4.30	0.817
EC:$BMIMBF_4$ = 9.13	1.840	4.07	0.812

On the other hand, in order to precisely adjust the interactions between BF_4^- and EC in the solutions, we gradually added 0.1 to 0.5 M $TEAPF_6$ into the 1.5 M $TEABF_4$-EC solution (FT-IR and Raman spectra are shown in Fig. S5a and b, ESI†). Since EC-solvated PF_6^- hardly intercalates into graphite electrodes, the AGICs formed in the above solutions may be only ascribed to EC-solvated BF_4^-. In other words, PF_6^- will seldom interfere with the solvated BF_4^-, which is already intercalated into graphite, but it exerts its impact out of the graphite electrode. As shown in the cyclic voltammograms of graphite electrodes in these solutions (Fig. 3), the addition of $TEAPF_6$ does take effect in suppressing the counter current. When the dose of $TEAPF_6$ reaches 0.3 M, the counter current disappears.

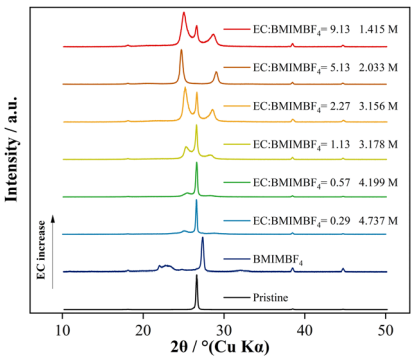

Fig. 2 *Ex situ* XRD patterns of graphite electrodes recovered from the AC/graphite cells charged to 3.5 V by utilizing the electrolyte of $BMIMBF_4$-EC.

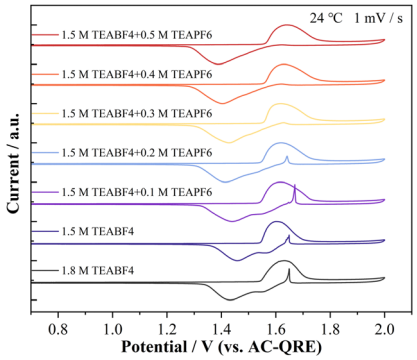

Fig. 3 Cyclic voltammograms of graphite electrodes in the electrolyte solutions of ($TEABF_4$ + $TEAPF_6$)-EC in the initial cycle.

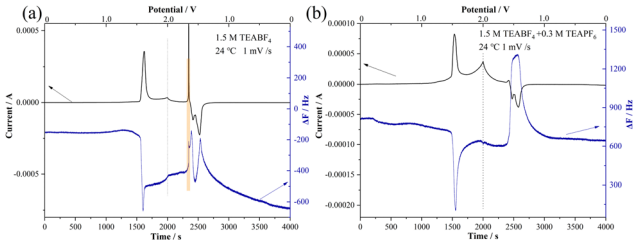

Fig. 4 CV–QCM curves of graphite electrode in the (a) 1.5 M $TEABF_4$-EC and (b) 1.5 M $TEABF_4$ + 0.3 M $TEAPF_6$-EC electrolyte solution.

To further address the instantaneous nature of counter-current, more *in situ* characterization is necessary. Herein EQCM (Schematic Diagram is shown in Fig. S6, ESI†) and ECD were chosen to capture this transient process. As shown in Fig. 4a, for the solution of 1.5 M $TEABF_4$-EC, during the charging process, the electrochemical intercalation gradually occurs and then generates anodic current as the potential climbs up. Meanwhile, the frequency of the quartz crystal electrode gradually decreases with the increase in current until the peak. According to the Sauerbrey equation, the corresponding electrode mass also reaches the maximum peak. Afterward, the concentration of BF_4^- on the graphite electrode surface decreases to 0, therefore, this electrochemical reaction is controlled by the anion diffusion inside the graphite. With an increase in potential, the diffusion layer gradually spreads out, and then the proceeding rate of anion intercalation becomes sluggish. If the charging process only involves BF_4^- intercalation, the mass of the graphite electrode must continue to increase, but at a decreasing pace. However, in reality, after the current reaches its maximum peak, the mass of the graphite electrode drops down quickly. This phenomenon corresponds to the mass loss during BF_4^- intercalation, which has been attributed to the release of some EC from the AGICs based on EC-solvated BF_4^-.[6,10] During discharge, a sharp anodic current peak jumps out at first along with the cathodic scan, and then follows two cathodic current peaks at lower potentials. Simultaneously, an anomalous increasing mass peak was observed in the frequency variation curve. This indicates the reverse entry of charged species into the graphite electrode during the deintercalation process, causing both mass and current-increasing responses. Consistent with our previous study,[6] the anion undergoes re-solvation when it deintercalates from graphite electrodes, resulting in the reflux of EC into the graphite. More importantly, BF_4^-, the charge carrier on the electrode surface, was driven back into graphite by the strong binding between the solvent and the anion, leading to the generation of counter current. As shown in Fig. 4b, the mass change during the charging process of the graphite electrode in the electrolyte containing $TEAPF_6$ is similar to that of 1.5 M $TEABF_4$-EC. However, there is no abnormal mass increase in the frequency variation curve during the discharge process. This can be attributed to the weakening of the interaction between BF_4^- and EC due to the addition of PF_6^-.

The ECD results will provide more insights into the switch-off of counter-current after introducing bits of $TEAPF_6$. As exhibited in Fig. 5a, the graphite electrode gradually expands from the voltage of about 2.5 V due to the continuous intercalation of anions in the 1.5 M $TEABF_4$-EC electrolyte. Subsequently, the thickness of the graphite decreases steadily during discharge. It is noteworthy that BF_4^- intercalates into graphite accompanied by EC on the electrode surface at approximately 2.8 V, which causes a tiny bulge of the ECD curve. On the contrary, there is no such sign in Fig. 5b. Conductivity of electrolyte, interface analyses, and kinetic analyses of graphite positive electrodes are shown in Fig. S7–S10, and Table S2 (ESI†).

It has been reported that the weakly polarized hydrogen atoms of C–H bonds can act as hydrogen bond donors for anions, especially when several such interactions work in concert.[11,12] Employment of electron withdrawing groups, such as a somewhat distant positive charge can reinforce these otherwise weak C–H···anion interactions.[13,14] We hypothesize that changes in the solvation structure of EC-BF_4^- by PF_6^- are eventuated from the different hydrogen bonding interactions. To verify it, ^1H–^{19}F 2D heteronuclear Overhauser effect spectroscopy (HOESY, whose signal strength is related to the spatial distance between the atoms) was employed to differentiate the interaction strengths between EC and BF_4^- or PF_6^-.[15,16] In order to maintain an equal total number of F atoms from both anions, our research focuses on a 0.9 M $TEABF_4$ + 0.6 M $TEAPF_6$-EC electrolyte solution as the experimental system. As

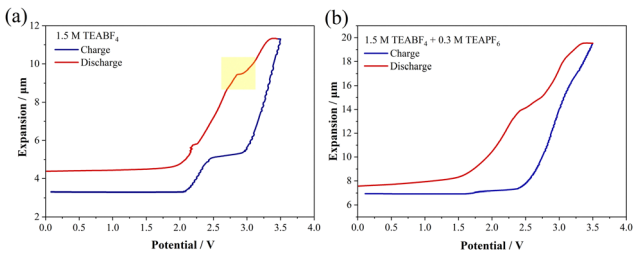

Fig. 5 ECD curves of graphite electrode in the (a) 1.5 M $TEABF_4$-EC and (b) 1.5 M $TEABF_4$ + 0.3 M $TEAPF_6$-EC electrolyte solution.

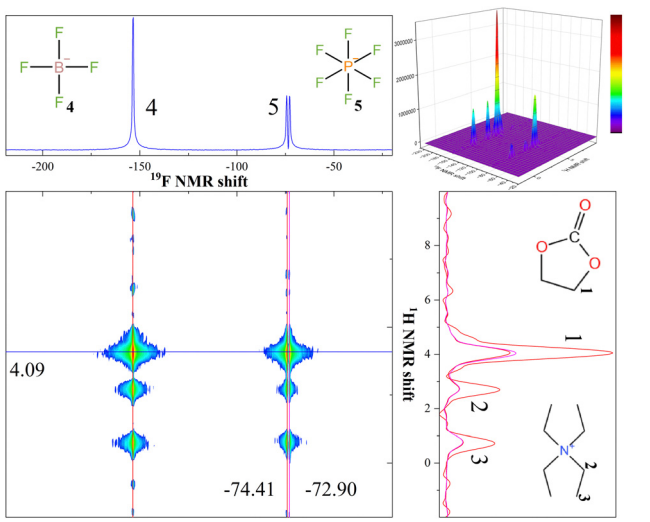

Fig. 6 ^1H–^{19}F HOESY spectra for the 0.9 M $TEABF_4$ + 0.6 M $TEAPF_6$-EC electrolyte solution.

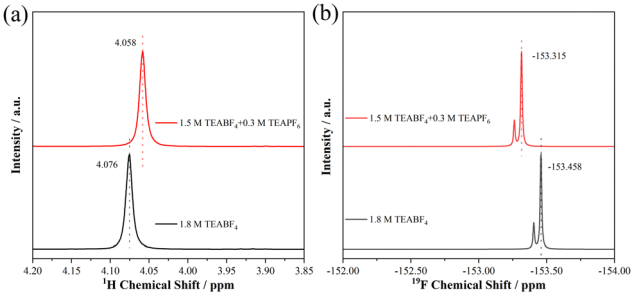

Fig. 7 (a) ^{1}H and (b) ^{19}F NMR spectra for the 1.5 M $TEABF_4$ + 0.3 M $TEAPF_6$-EC and 1.8 M $TEABF_4$-EC solutions.

shown in the ^{19}F horizontal trace projection of the contour map of Fig. 6, the signals of BF_4^- and PF_6^- located at −153.6 and −72.9 ppm, respectively.[16,17] As for ^{1}H, both EC solvents and TEA^+ cations appear in the vertical trace projection of the contour map of Fig. 6.[18] Herein, the interaction between anions and solvents can be compared qualitatively in terms of the intensity of the cross peak. ^{1}H atoms in EC approach ^{19}F of BF_4^- and exhibit a stronger relation to it instead of PF_6^-. Therefore, it can be foreseen that the interaction of the hydrogen bonding network will be weakened, when some PF_6^- partially replaces BF_4^- around the EC. So as to confirm it, further investigation was conducted on the ^{1}H and ^{19}F NMR spectra for the 1.8 M $TEABF_4$-EC and 1.5 M $TEABF_4$ + 0.3 M $TEAPF_6$-EC solutions shown in Fig. 7a and b. While total concentration is controlled at 1.8 M, the chemical shift of ^{1}H in EC moves upfield in the 0.3 M $TEAPF_6$ + 1.5 M $TEABF_4$, indicating an increase in electron cloud density and a stronger shielding effect around the H nuclei of EC. Additionally, the chemical shift of ^{19}F moves downfield, suggesting a decrease in electron cloud density around the F nuclei of BF_4^-, which implies weakened interaction between the F anions and the solvent H atoms. Given the potential influence of higher concentrations of salt on the manifestation of C–H···anion interactions in the NMR spectra, which result from the presence of contact ion pairs and aggregates, we chose to employ a lower electrolyte concentration of 1 M to ensure sufficient solvent for electrolyte dissociation, as shown in Fig. S11 (ESI†). As the concentration of PF_6^- increases, the chemical shift of ^{1}H in EC moves towards upfield, while the strength of C–H···anion interactions decreases. It also supports the aforementioned conclusion. The addition of PF_6^- weakens the interaction of EC-BF_4^-, making it challenging for EC to effectively capture BF_4^- during its reverse flow into the graphite.

In summary, the electrochemical processes of anion intercalation and deintercalation in graphite electrodes are greatly influenced by their solvation state. The storage behavior of BF_4^- inside the graphite cathode varies with the molar ratios of [$BMIMBF_4$]/[EC] in the corresponding electrolyte solutions. The back-flows of EC solvent from the electrolyte solution into the graphite electrode, in conjunction with the strong affinity between EC and the anion, result in the generation of a counter-current during BF_4^- deintercalation. NMR spectra have confirmed that this strong affinity originates from solvent-anion hydrogen bonding interactions. By introducing PF_6^- into the electrolyte, the counter current was successfully controlled through the modulation of long-range interaction between anion and solvent. In addition, another electrolyte was also studied to investigate the universality of the counter-current (Fig. S12, ESI†). Anion solvation in electrolytes can change the electrochemical performance of the electrolytes, but it has been rarely investigated. This unexplored area has begun to show its potential in rational electrolyte design for lithium metal batteries[19,20] and is also anticipated to bring unique insights into the field of dual-ion batteries involving anion participation in intercalation.

This work was financially supported by the National Key R&D Program of China (2022YFB2402600).

Data availability

The data supporting this article have been included as part of the ESI.†

Conflicts of interest

There are no conflicts to declare.

References

1 H. Guo, M. Elmanzalawy, P. Sivakumar and S. Fleischmann, *Energy Environ. Sci.*, 2024, **17**, 2100.
2 J. Li, C. Han, X. Ou and Y. Tang, *Angew. Chem., Int. Ed.*, 2022, **61**, e202116668.
3 Z. Zhao and H. N. Alshareef, *Adv. Mater.*, 2024, **36**, 2309223.
4 X. Tong, X. Ou and Y. Tang, *Adv. Energy Mater.*, 2021, **11**, 2100151.
5 J. Lang, Y. Liu and Y. Tang, *Small*, 2024, 2401200.
6 Y. Huang, J. Li and H. Wang, *ACS Appl. Energy Mater.*, 2019, **2**(6), 4544–4550.
7 D. Zhu, L. Zhang, Y. Huang, J. Li, H. Fan and H. Wang, *ACS Appl. Energy Mater.*, 2019, **2**(11), 8031–8038.
8 P. W. Ruch, D. Cericola, M. Hahn, R. Kotz and A. Wokaun, *J. Electroanal. Chem.*, 2009, **636**, 128–131.
9 M. S. Dresselhaus and G. Dresselhaus, *Adv. Phys.*, 1981, **30**(2), 139–326.
10 J. Gao, M. Yoshio, L. Qi and H. Wang, *J. Power Sources*, 2015, **278**, 452–457.
11 Y. J. Li and A. H. Flood, *Angew. Chem., Int. Ed.*, 2008, **47**, 2649–2652.
12 B. J. J. Timmer and T. J. Mooibroek, *Chem. Commun.*, 2021, **57**, 7184–7187.
13 J. J. Cai and J. L. Sessler, *Chem. Soc. Rev.*, 2014, **43**, 6198–6213.
14 B. W. Tresca, R. J. Hansen, C. V. Chau, B. P. Hay, L. N. Zakharov, M. M. Haley and D. W. Johnson, *J. Am. Chem. Soc.*, 2015, **137**, 14959–14967.
15 I. Fernandez and P. S. Pregosin, *Magn. Reson. Chem.*, 2006, **44**, 76–82.
16 Y. Wang, J. Li, Y. Huang and H. Wang, *Langmuir*, 2019, **35**(46), 14804–14811.
17 M. Nie, D. Chaalasani, D. P. Abraham, Y. Chen, A. Bose and B. L. Lucht, *J. Phys. Chem. C*, 2013, **117**(3), 1257–1267.
18 C. Jehanno, J. Demarteau and H. Sardon, *Angew. Chem., Int. Ed.*, 2021, **60**, 6710–6717.
19 J. Xu, V. Koverga, A. Phan, A. M. Li, N. Zhang, M. Baek, C. Jayawardana, B. L. Lucht, A. T. Ngo and C. Wang, *Adv. Mater.*, 2024, **36**, 2306462.
20 Y. Tian, S. Tan, Z. Lu, D. Xu, H. Chen, C. Zhang, X. Zhang, G. Li, Y. Zhao, W. Chen, Q. Xu, R. Wen, J. Zhang and Y. Guo, *Angew. Chem., Int. Ed.*, 2023, **62**, e202305988.

